

# Contact resistance and shot noise in graphene transistors

J. Cayssol

CPMOH, UMR 5798, Université de Bordeaux,  
33405 Talence, France

B. Huard\* and D. Goldhaber-Gordon

Stanford University, Department of Physics, Stanford, California, USA

Potential steps naturally develop in graphene near metallic contacts. We investigate the influence of these steps on the transport in graphene Field Effect Transistors. We give simple expressions to estimate the voltage-dependent contribution of the contacts to the total resistance and noise in the diffusive and ballistic regimes.

Graphene's distinctive band structure gives rise to exciting new transport properties and promising applications for carbon-based electronics<sup>1,2,3</sup>. When measuring the conductance or current noise in a nanotube or a sheet of graphene, the properties of the contacts can matter as much as the electronic structure of the nanotube or graphene itself. In semiconducting nanotubes or graphene nanoribbons, it is known that Schottky barriers develop at the metallic contacts<sup>4,5</sup>. Charge transfer between a metal and a wide graphene strip induces potential steps whose shape may differ strongly from usual Schottky barriers due to the semimetallic and two-dimensional nature of graphene. The existence of such metal-induced potential steps was inferred experimentally from the transport properties of a graphene strip with various contact geometries<sup>6</sup>. More direct evidence for these steps comes from optical mapping of the potential landscape across a graphene device<sup>7</sup>. Recent theoretical work on graphene-metal interfaces has been performed within the atomistic tight-binding theory<sup>8,9</sup>.

In this paper, the conductance and the shot noise of graphene Field Effect Transistors (gFETs) with extended contacts are derived using the Dirac Hamiltonian for graphene. Near a single contact, we assume that the Fermi energy in graphene varies monotonically over a characteristic length  $d$ , and we solve the corresponding scattering problem exactly. If the transport is ballistic between both contacts, we predict oscillations of the noise and conductance as the charge density is increased in the sheet. When the density exceeds the one under the contact, the noise minima might be zero and correspond to perfect transmission between the contacts. Such realizations of a noiseless gFET are caused by Fabry-Pérot resonances and require low doping by the contacts. In the diffusive regime, we show how the total resistance and Fano Factor of the whole gFET depend upon the contact resistance and Fano factor of each contact, which is relevant in interpreting recent experiments on shot noise in non-suspended graphene<sup>10,11</sup>.

Before analyzing the gFETs' properties, it is useful to investigate transport across a single graphene-metal contact. We thus consider that a metal electrode covers the left half-plane ( $x < 0$ ) of an infinite graphene layer. We assume that the metal coating simply shifts

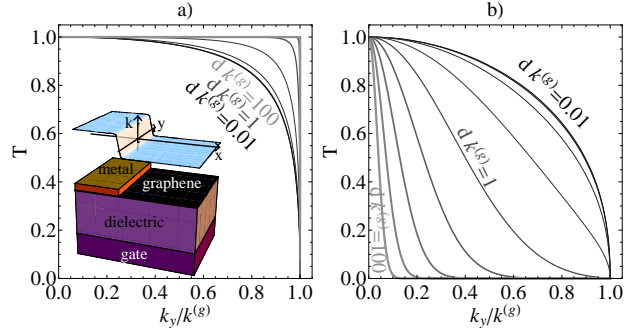


FIG. 1: a) Transmission probability  $\mathcal{T}_{\text{step}}$  across the metal/graphene interface as a function of transverse momentum  $k_y$  for several lengths  $d$  of the potential rise. The ratio between Fermi wavevectors in bulk graphene and below the metal is set to  $k_F^{(m)}/k_F^{(g)} = 3$  (unipolar contact). A schematic of the device and corresponding Fermi wavevector profile  $k_F(x)$  are shown in the inset. b) same curves for a bipolar contact with  $k_F^{(m)}/k_F^{(g)} = -3$ .

the Fermi level of the graphene underneath while preserving its pristine Dirac cones<sup>12</sup>. Far from the contact, the type ( $n$  or  $p$ ) and density of charge carriers in the right half-plane ( $x > 0$ ) are tuned by a distant metallic gate. A continuous Fermi wave vector profile  $k_F(x)$  must therefore develop near the contact edge to match the asymptotic values  $k_F(-\infty) = k_F^{(m)}$  under the metal, and  $k_F(+\infty) = k_F^{(g)}$  in bare graphene. The dynamics of the massless fermions can be safely described by the single-valley two-dimensional Dirac Hamiltonian,

$$H = -i\hbar v_F [\sigma_x \partial_x + \sigma_y \partial_y - ik_F(x)\mathbf{1}], \quad (1)$$

which is valid if the potential step is smooth on the scale of the lattice constant. Here  $v_F$  is the Fermi velocity and

$$k_F(x) = k_F^{(m)} + \frac{k_F^{(g)} - k_F^{(m)}}{e^{-x/d} + 1} \quad (2)$$

our simple model for the space-dependent Fermi wave vector (Fig. 1 inset). The Pauli matrices  $(\sigma_x, \sigma_y, \sigma_z)$  operate on spinors  $\Psi(x, y)$  whose components are the electron amplitudes associated with each sublattice of the

honeycomb carbon crystal. It is worthy to note that a complete treatment of nonlinear screening and disorder near the contact should lead to a more complicated profile in the bipolar  $n$ - $p$  case<sup>14,15</sup>. Nevertheless this can be accounted for by noting that our phenomenological  $d$  will in fact depend on  $k_F^{(m)}$  and  $k_F^{(g)}$  in a way that may ultimately be calculated.

We now proceed to the derivation of simple formulas relating the transport properties (as functions of  $k_F^{(g)}$ ) to the parameters  $d$  and  $k_F^{(m)}$  characterizing the contacts. Here we consider a wide enough graphene strip to neglect edge effects<sup>16</sup>. Then translational invariance parallel to the junction (along the  $y$  axis) implies that the transverse wavevector  $k_y$  is conserved, and all spinor wavefunctions take the form  $\Psi(x, y) = \Phi(x)e^{ik_y y}$  where  $\Phi(x) = {}^T(\Phi_1(x), \Phi_2(x))$ . Aiming to determine the low temperature transport, we solve the Dirac equation at the Fermi level ( $H\Psi(x, y) = 0$ ) which reduces to the one-dimensional equation

$$\partial_x \Phi(x) = (k_y \sigma_z + ik_F(x) \sigma_x) \Phi(x). \quad (3)$$

This equation can be decoupled using the symmetric/antisymmetric combinations of components  $f_{\pm}(x) = \Phi_1(x) \pm \Phi_2(x)$  which obey the following scalar differential equations:

$$f_{\alpha}'' + (k_F^2(x) - k_y^2 - i\alpha k_F'(x)) f_{\alpha} = 0, \quad (4)$$

where  $\alpha = \pm$ . In the asymptotic regions  $|x| \gg d$ , the solutions are plane waves  $f_{\alpha}(x) = e^{\pm ik_x x}$  which can be either exponentially damped or oscillatory depending on the sign of  $k_x^2 = k_F^2 - k_y^2$ . In order to find the transmission across the potential step Eq. (2), we now construct a scattering state containing a single oscillatory outgoing charge state (with  $|k_y| < |k_F^{(g)}|$ ) in the region  $x \rightarrow +\infty$ , namely

$$f_{\alpha}(x) \sim e^{ik_x^{(g)} x} \text{ at } x \rightarrow +\infty. \quad (5)$$

Here  $k_x^{(g)} = s_g \sqrt{(k_F^{(g)})^2 - k_y^2}$  is the longitudinal momentum whose direction depends on the band index  $s_g = \text{sign}(k_F^{(g)})$  far on the right side. In Appendix A, we show that this asymptotic condition completely determines the solution of the Dirac equation  $H\Psi(x, y) = 0$  on the whole  $x$ -axis. In particular, on the left side the wave consists of a superposition

$$f_{\alpha}(x) \sim f_{\alpha}^{(inc)}(x) + f_{\alpha}^{(ref)}(x) \text{ at } x \rightarrow -\infty, \quad (6)$$

of an incoming

$$f_{\alpha}^{(inc)}(x) = \frac{\Gamma(1 - 2ik_x^{(g)}d)\Gamma(-2ik_x^{(m)}d)}{\Gamma(i\kappa^{-}d)\Gamma(1 - i\kappa^{+}d)} e^{ik_x^{(m)}x}, \quad (7)$$

and a reflected charge carrier

$$f_{\alpha}^{(ref)} = \frac{\Gamma(1 - 2ik_x^{(g)}d)\Gamma(2ik_x^{(m)}d)}{\Gamma(i\kappa^{-}d)\Gamma(1 - i\kappa^{+}d)} e^{-ik_x^{(m)}x}. \quad (8)$$

Here  $k_x^{(m)} = s_m \sqrt{(k_F^{(m)})^2 - k_y^2}$  and  $s_m = \text{sign}(k_F^{(m)})$  indicates whether graphene is  $n$ - or  $p$ -doped underneath the metal. The Euler Gamma function is denoted  $\Gamma(z)$  and we have introduced the momenta  $\kappa^{\rho\sigma} = k_F^{(g)} - k_F^{(m)} + \rho k_x^{(g)} + \sigma k_x^{(m)}$ , with  $\rho, \sigma = \pm 1$ . The corresponding reflection probability is simply given by

$$\mathfrak{R}_{\text{step}} = \left| \frac{\Gamma(1 - i\kappa^{++}d)\Gamma(i\kappa^{--}d)}{\Gamma(1 - i\kappa^{+-}d)\Gamma(i\kappa^{-+}d)} \right|^2 \quad (9)$$

when all the waves are propagating, namely for  $|k_y| < \min(|k_F^{(g)}|, |k_F^{(m)}|)$ . Finally, a remarkably simple formula is obtained for the reflection coefficient of Dirac fermions across the potential step Eq. (2):

$$\mathfrak{R}_{\text{step}} = \frac{\sinh(\pi d \kappa^{+-}) \sinh(\pi d \kappa^{-+})}{\sinh(\pi d \kappa^{++}) \sinh(\pi d \kappa^{--})}. \quad (10)$$

This expression is valid for any  $d$  and step polarity, matching the known limits for transport across smooth<sup>17</sup> and abrupt ( $d \rightarrow 0$ ) steps<sup>18</sup>, and interpolating between those limits. The expression (10) is reminiscent of the reflection coefficient of a non-relativistic massive scalar particle,  $\mathfrak{R} = \sinh(\pi d |k_x^{(g)} - k_x^{(m)}|) / \sinh(\pi d |k_x^{(g)} + k_x^{(m)}|)$ , obtained by solving the Schrödinger equation in a similar potential landscape<sup>13</sup>. The richer structure of Eq. (10) is associated with the Dirac nature of carriers in graphene. In particular, it indicates the absence of backscattering at normal incidence ( $k_x^{(m,g)} = k_F^{(m,g)}$ ) for any height and width of the potential step, which is related to the orthogonality of incoming and reflected spinor states<sup>19</sup>. As with standard impedance matching, the transmission

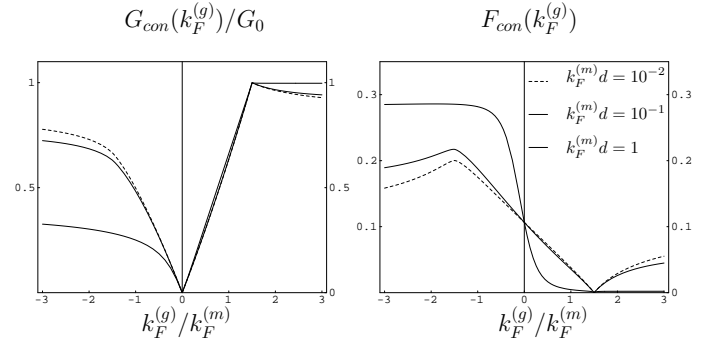


FIG. 2: Contact conductance (left) and Fano factor (right) associated with a single potential step as functions of the Fermi wavevector in bulk graphene  $k_F^{(g)}$  for several values of the dimensionless parameter  $k_F^{(m)}d$ . The maximal value of the conductance is given by  $G_0 = 4e^2 N/h$  where  $N = k_F^{(m)}W/\pi$ .

$\mathcal{T}_{\text{step}} \equiv 1 - \mathfrak{R}_{\text{step}}$  of the unipolar contact tends toward unity when the distance  $d$  is increased (Fig. 1). In contrast, for bipolar steps, the  $k_y$ -dependent transmission  $\mathcal{T}_{\text{step}}$  goes from a broad curve at small  $d$  to a sharp peak around  $k_y = 0$  at large  $d$  (Fig. 1). Besides, the bipolar

transmission counter-intuitively increases when the potential barrier height is increased. Although the potential step originates from charge transfer between a metal and graphene, these scattering properties are similar to the relativistic Klein tunneling<sup>20</sup> for which evidence is mounting in the context of transport through potential barriers created by local gates<sup>15,21,22,23,24,25,26</sup>.

From the transmission probability  $\mathcal{T}_{\text{step}}$ , the conductance and the Fano factor of a single contact are given respectively by

$$G_{\text{con}}(k_F^{(g)}) = \frac{4e^2}{h} \frac{W}{2\pi} \int_{-k_F^{(m)}}^{k_F^{(m)}} \mathcal{T}_{\text{step}} dk_y, \quad (11)$$

and

$$F_{\text{con}}(k_F^{(g)}) = \int_{-k_F^{(m)}}^{k_F^{(m)}} dk_y \mathcal{T}_{\text{step}} (1 - \mathcal{T}_{\text{step}}) / \int_{-k_F^{(m)}}^{k_F^{(m)}} dk_y \mathcal{T}_{\text{step}},$$

where  $W$  is the width of the graphene strip along  $y$  and  $k_F^{(g)}$  is related to the asymptotic density  $n^{(g)}$  at  $x \gg d$  by the relation  $k_F^{(g)} = \sqrt{\pi n^{(g)}}$ . These quantities are strongly sensitive to the nature and density of charge carriers (Fig. 2). The bipolar contact is clearly more resistive and noisier than the unipolar one, and this unipolar/bipolar asymmetry becomes more pronounced for smoother contacts (Fig. 2). In the limit of very smooth potential steps ( $k_F^{(m)}d \rightarrow \infty$ ), the Fano factor vanishes in the unipolar case whereas it saturates to a finite value  $F_{\text{con}}(k_F^{(g)} < 0) = 1 - 2^{-1/2}$  in the bipolar case (in agreement with<sup>17</sup>). As expected a single contact becomes noiseless when the potential step vanishes ( $k_F^{(g)} = k_F^{(m)}$ ). In the sequel of the paper, we use the result Eq. (10) to investigate the effect of the contact potential steps<sup>6,7</sup> on the conductance and noise properties of gFETs.

Recently, suspended gFETs have been achieved, resulting in increased mobility of the two-dimensional electron gas<sup>27,28,29</sup>. In such devices electronic motion might become ballistic between source and drain. The whole structure can be described by two symmetric steps similar to Eq. (2) and separated by a distance  $L$ , the so-called Wood-Saxon potential Eq. (B1). The single channel transmission exhibits Fabry-Pérot-like resonances as the gate voltage varies. We calculate the transmission probability using a mapping between the problem of massless Dirac fermions in graphene and the one of massive Dirac fermions in the one-dimensional Wood-Saxon potential<sup>31</sup>. The contrast of the whole interference pattern is controlled by the reflection probability  $\mathfrak{R}_{\text{step}}(k_y)$  which depends strongly on the distance  $d$ , as discussed above, see Eq. (10).

In the large gate voltage regime,  $|k_F^{(g)}| > |k_F^{(m)}|$ , the wavefunctions are oscillatory for all transverse channels, and the corresponding transmission across the whole de-

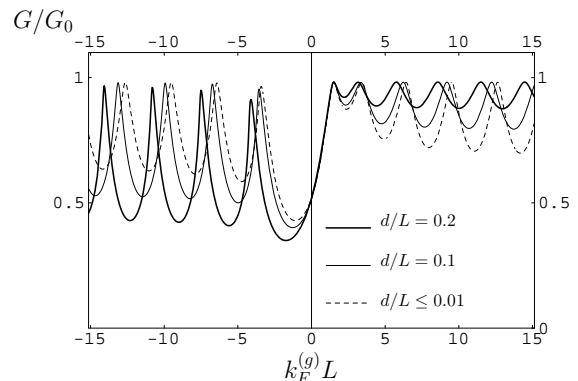


FIG. 3: Conductance  $G$  of a ballistic Fabry-Pérot cavity as a function of the dimensionless parameter  $k_F^{(g)}L$ . The maximal conductance ( $G_0 = 4e^2N/h$ ) is controlled by the number of available propagating modes in the leads  $N = k_F^{(m)}W/\pi$ . Here  $k_F^{(m)}L = 1.5$ , which means  $L = 27$  nm for a density  $n^{(m)} = 10^{11}$  cm<sup>-2</sup>, and the aspect ratio  $W/L$  is large (in practice  $W/L \gtrsim 4$  is sufficient<sup>16</sup>). For definiteness, we have assumed that the graphene is  $n$ -doped underneath the metal ( $k_F^{(m)} > 0$ ). In this case, the minimal conductivity is reached at a nonzero negative density in the central channel. For other metals that produce  $p$ -doped graphene after charge transfert, one should obtain the symmetrical curves (with respect to vertical axis  $k_F^{(g)}L = 0$ ) of the ones presented here, and the shift of the minimal conductivity would occur at positive density.

vice can be approximated by

$$\mathcal{T}_{\text{ball}}(k_y) \approx \left( 1 + \frac{4\mathfrak{R}_{\text{step}}(k_y)}{(1 - \mathfrak{R}_{\text{step}}(k_y))^2} \sin^2(k_x^{(g)}L) \right)^{-1} \quad (12)$$

when neglecting the corrections of order  $d$  to the effective size of the cavity. The shape of the cavity enters this formula through the reflection probability  $\mathfrak{R}_{\text{step}}(k_y)$ . The actual position of the conductance peaks (Fig. 3) is modified because the effective width of the cavity changes with  $d$ . In this regime, the conductance of realistic cavities is globally smaller (Fig. 3) than the prediction of the square well-model ( $d = 0$ ) with infinite doping below the electrodes ( $k_F^{(m)} = \infty$ )<sup>30</sup>. Indeed the maximal conductance ( $4e^2N/h$ ) is controlled by the number of available propagating modes in the leads  $N = k_F^{(m)}W/\pi$  as soon as the doping of the two-dimensional electron gas in the middle part of the gFET exceeds that underneath the source and drain contacts. At large absolute gate voltages ( $k_F^{(g)} < -k_F^{(m)}$ ), the bipolar conductance exhibits strong oscillations whose contrast increases as the steps become smoother (Fig. 3). In contrast at  $k_F^{(g)} > k_F^{(m)}$ , the unipolar cavity becomes fully transparent in the large  $d$  limit wherein the oscillations are lost. Similar fringes have already been observed recently in short Fabry-Pérot devices created by local gating<sup>29</sup>. We suggest making contacts with a metal which dopes the graphene very lightly in order to observe the Fabry-Pérot interferences with the highest resolution in bipolar cavities.

We now discuss the more usual low gate voltage regime  $|k_F^{(g)}| < |k_F^{(m)}|$ , wherein the conductance is determined by both evanescent and propagating modes. Besides being nonuniversal, the minimal conductance is reached at nonzero carrier density  $n_{\min}^{(g)} \neq 0$ . Up to now, the minimum conductance was predicted to occur at a non-zero gate voltage (due to charge impurities) but at zero average density<sup>35</sup>. Here, we predict that the presence of metallic contacts can shift this minimum to non-zero charge density, even without impurities. Besides, the

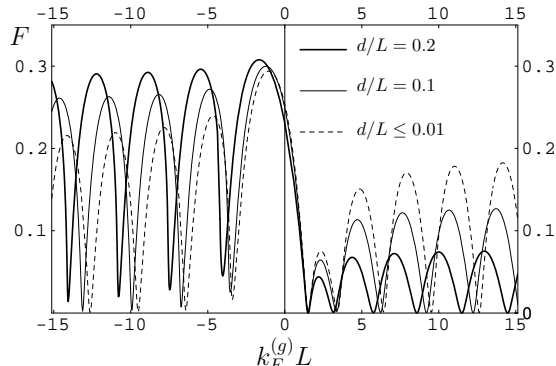


FIG. 4: Fano factor for a ballistic graphene Fabry-Pérot cavity as a function of the dimensionless parameter  $k_F^{(g)}L$  for various values of  $d/L$ . Same parameters as in Fig. 3, in particular  $k_F^{(m)}L = 1.5$  while the aspect ratio  $W/L$  is large<sup>16</sup>, namely  $W/L \gtrsim 4$ .

Fabry-Pérot interferences should also induce signatures on the noise of clean gFETs. Here we demonstrate that the Fano factor of a ballistic gFET,

$$F_{\text{ball}}(k_F^{(g)}) = \frac{\int dk_y \mathcal{T}_{\text{ball}}(1 - \mathcal{T}_{\text{ball}})}{\int dk_y \mathcal{T}_{\text{ball}}}, \quad (13)$$

should exhibit spectacular oscillations as a function of the dimensionless parameter  $k_F^{(g)}L$  (Fig. 4) for cavities operated at gate voltages yielding  $|k_F^{(g)}| > k_F^{(m)}$ . In particular for  $k_F^{(g)} > k_F^{(m)}$ , the Fano factor shows successive nodes at the gate voltages corresponding to peaks of optimal conductance (Fig. 3). On the bipolar side  $k_F^{(g)} < -k_F^{(m)}$ , the nodes are replaced by local minima of  $F_{\text{ball}}$  corresponding to local maxima of the conductance. These oscillations have not been investigated either experimentally or theoretically. Early theoretical works assumed infinite doping by the contacts<sup>30</sup>.

We now consider the situation, relevant to non-suspended gFETs, where the carrier motion is diffusive between the source and the drain. Assuming phase-incoherent transport, the total resistance of the gFET is simply given by  $R_{\text{dif}} = R_{\text{sheet}}(k_F^{(g)}) + 2R_{\text{con}}(k_F^{(g)})$  and the Fano factor by<sup>36</sup>

$$F_{\text{dif}}(k_F^{(g)}) = \frac{2R_{\text{con}}^2 F_{\text{con}} + R_{\text{sheet}}^2 F_{\text{sheet}}}{(2R_{\text{con}} + R_{\text{sheet}})^2}, \quad (14)$$

where  $R_{\text{sheet}}$  and  $F_{\text{sheet}}$  are respectively the resistance and the Fano factor of the sheet, and  $R_{\text{con}} = G_{\text{con}}^{-1}$  the single contact resistance. Theory of the anomalous diffusion through the electron-hole puddles sea formed in graphene predicts a universal scale-independent Fano factor  $F_{\text{sheet}} = 1/3$ <sup>32</sup> in agreement with a recent experiment<sup>10</sup>. In addition numerical studies also indicate a nearly density independent Fano factor (not universally equal to 1/3) from moderate to strong disorder<sup>33,34</sup>. According to Eq. (14), one expects  $F_{\text{dif}}(k_F^{(g)}) = F_{\text{sheet}} = 1/3$  only when  $R_{\text{sheet}} \gg R_{\text{con}}$  which might be the case in all devices measured in Ref.<sup>10</sup>. In contrast, when  $R_{\text{sheet}} \ll R_{\text{con}}$ ,  $F_{\text{dif}}(k_F^{(g)})$  depends more on  $F_{\text{con}}$  which makes it decrease as a function of  $|k_F^{(g)}|$ . Interestingly another experiment reports on such a decrease from  $F_{\text{dif}}(k_F^{(g)} = 0) = 1/3$  to a lower value at large densities<sup>11</sup>. Nevertheless it should be emphasized that the incoherent theory underlying Eq.(14) is not valid for the very short graphene devices investigated in Ref.<sup>11</sup>. It is thus necessary to consider the nonlocal transport properties of the whole device. Unfortunately the precise profile of the potential in this experiment is not known and probably corresponds to  $L \sim d$  making neither our study of the ballistic Fabry-Pérot (Fig. 4) nor the square well model of Ref.<sup>30</sup> quantitatively relevant. Nevertheless the qualitative behavior of these experiments is captured by these models: intrinsic noise close to the Dirac point and contact-dominated noise at larger densities.

In conclusion, we have considered Dirac fermions scattering from one or two potential steps having each a characteristic length  $d$ . Such steps introduce additional dissipation localized at the source and drain of gFETs and also modify drastically the noise properties of such devices. In the ballistic regime, we predict that the presence of metallic contacts can shift the conductance minimum to a non-zero charge density, which is negative (resp. positive) for a metal which dopes the graphene with electrons (resp. with holes). In addition we also suggest performing conductance and noise measurements on a suspended bipolar graphene Fabry-Pérot structure<sup>27,28,29</sup> with low doping at the electrodes in order to observe enhanced Fabry-Pérot oscillations. Finally, the asymmetry between electron and hole transport is enhanced when these potential steps rise over longer distances.

## APPENDIX A: TRANSMISSION ACROSS A POTENTIAL STEP

We consider the differential equation Eq.(4):

$$f''_{\alpha} + (k_F^2(x) - k_y^2 - \alpha i k_F'(x))f_{\alpha} = 0, \quad (A1)$$

where

$$k_F(x) = k_F^{(m)} + \frac{k_F^{(g)} - k_F^{(m)}}{e^{-x/d} + 1}. \quad (A2)$$

We introduce the new independent variable  $\xi = -e^{-x/d}$  and seek for the solutions in the general form  $f_\alpha(x) = \xi^\mu(1-\xi)^{-\lambda}w_\alpha(\xi)$ . The function  $w_\alpha(\xi)$  satisfies the Gauss hypergeometrical equation:

$$\xi(1-\xi)w_\alpha'' + [c - (a+b+1)\xi]w_\alpha' - abw_\alpha = 0, \quad (\text{A3})$$

if the exponents are chosen as

$$\mu = -ik_x^{(g)}d \quad \text{and} \quad \lambda = -i(k_F^{(g)} - k_F^{(m)})d. \quad (\text{A4})$$

Introducing  $\nu = ik_x^{(m)}d$ , the parameters  $a, b, c$  are given by

$$c = 1 + 2\mu, \quad (\text{A5})$$

$$a + b + 1 = 1 + 2\mu - 2\lambda, \quad (\text{A6})$$

$$a = (\mu - \lambda + \nu), \quad (\text{A7})$$

$$b = (\mu - \lambda - \nu). \quad (\text{A8})$$

In the region  $x \rightarrow +\infty$ , namely  $\xi \rightarrow 0$ , the two independent solutions of the hypergeometric equation are  $w_\alpha(\xi) = F(a, b, c; \xi)$  and  $w_\alpha(\xi) = \xi^{1-c}F(a-c+1, b-c+1, 2-c; \xi)^{37}$ . The corresponding functions  $f_\alpha(x) = \xi^\mu w_\alpha(\xi)$  are the plane waves  $\xi^\mu = e^{ik_x^{(g)}d}$  and  $\xi^{-\mu} = e^{-ik_x^{(g)}d}$ . We now construct a scattering state containing a single oscillatory outgoing wave in the region  $x \rightarrow +\infty$ , namely

$$f_\alpha(x) \sim e^{ik_x^{(g)}x} \text{ at } x \rightarrow +\infty, \quad (\text{A9})$$

where  $k_x^{(g)} = s_g \sqrt{(k_F^{(g)})^2 - k_y^2}$  is the longitudinal momentum whose direction depends on the band index  $s_g = \text{sign}(k_F^{(g)})$  far on the right side. Note that although the sign of  $k_x^{(g)}$  can be either positive or negative depending on doping, the group velocity always describes a right-moving charge.

From the general relation<sup>37</sup> between the hypergeometric functions of respective arguments  $\xi$  and  $1/\xi$ , one can extract the asymptotic behavior of  $w(\xi)$  in the region for  $\xi \rightarrow -\infty$

$$w_\alpha(\xi) = \frac{\Gamma(c)\Gamma(b-a)}{\Gamma(b)\Gamma(c-a)}(-\xi)^{-a} \quad (\text{A10})$$

$$+ \frac{\Gamma(c)\Gamma(a-b)}{\Gamma(a)\Gamma(c-b)}(-\xi)^{-b}. \quad (\text{A11})$$

Consequently the structure of the wave  $f_\alpha(x) = \xi^\mu(1-\xi)^{-\lambda}w(\xi) \sim \xi^\mu(-\xi)^{-\lambda}w(\xi)$  in the region  $x \rightarrow -\infty$  (namely  $\xi \rightarrow -\infty$ ) consists in two parts

$$f_\alpha(x) \sim f_\alpha^{(inc)}(x) + f_\alpha^{(ref)}(x) \text{ at } x \rightarrow -\infty, \quad (\text{A12})$$

which are respectively the incident wave

$$f_\alpha^{(inc)}(x) = (-1)^\mu \frac{\Gamma(c)\Gamma(b-a)}{\Gamma(b)\Gamma(c-a)} e^{ik_x^{(m)}x}, \quad (\text{A13})$$

and the reflected wave

$$f_\alpha^{(ref)} = (-1)^\mu \frac{\Gamma(c)\Gamma(a-b)}{\Gamma(a)\Gamma(c-b)} e^{-ik_x^{(m)}x}. \quad (\text{A14})$$

We have used

$$(-\xi)^{-a+\mu-\lambda} = (e^{-x/d})^{-\nu} = e^{ik_x^{(m)}x} \quad (\text{A15})$$

$$(-\xi)^{-b+\mu-\lambda} = (e^{-x/d})^\nu = e^{-ik_x^{(m)}x} \quad (\text{A16})$$

We emphasize again that  $e^{ik_x^{(m)}x}$  is always the right-moving incident wave, although  $k_x^{(m)}$  can be either positive or negative (because the projection of the group velocity is positive in both n-type and p-type doped graphene). Therefore the reflection probability is:

$$\mathfrak{R}_{\text{step}} = \left| \frac{\Gamma(b)\Gamma(c-a)}{\Gamma(a)\Gamma(c-b)} \right|^2 \quad (\text{A17})$$

$$= \left| \frac{\Gamma(\mu-\lambda-\nu)\Gamma(1+\lambda+\mu-\nu)}{\Gamma(\mu-\lambda+\nu)\Gamma(1+\lambda+\mu+\nu)} \right|^2 \quad (\text{A18})$$

which leads to Eqs.(9,10) in the text.

## APPENDIX B: WOOD-SAXON POTENTIAL

The Wood-Saxon potential corresponds to two symmetric steps

$$k_F(x) = k_F^{(m)} + \left( k_F^{(g)} - k_F^{(m)} \right) \times \left( \frac{\theta(-x)}{e^{-(x+L/2)/d} + 1} + \frac{\theta(x)}{e^{(x-L/2)/d} + 1} \right) \quad (\text{B1})$$

We have checked that the transmission probability is given by the formula of Ref.<sup>31</sup>, namely  $\mathcal{T}_{\text{ball}}(k_y) = |Ae^{\mu L/d} / (1 - Ce^{2\mu L/d})|^2$  where

$$A = \left( \frac{(\mu + \nu)^2 - \lambda^2}{4\mu\nu} \right) \quad (\text{B2})$$

$$\frac{\Gamma^2(-\mu - \nu - \lambda)\Gamma^2(-\mu - \nu + \lambda)}{\Gamma^2(-2\mu)\Gamma^2(-2\nu)}, \quad (\text{B3})$$

$$C = \left[ \frac{(\mu + \nu)^2 - \lambda^2}{(\mu - \nu)^2 - \lambda^2} \right] \frac{B^2(2\mu, -\mu - \nu + \lambda)}{B^2(-2\mu, \mu - \nu - \lambda)}. \quad (\text{B4})$$

We denote  $B(a, b) = \Gamma(a)\Gamma(b)/\Gamma(a+b)$  the beta function, and  $\mu = -ik_x^{(g)}d$ ,  $\nu = ik_x^{(m)}d$ ,  $\lambda = -i(k_F^{(g)} - k_F^{(m)})d$  like in appendix A.

## ACKNOWLEDGMENTS

We are very grateful to Bjoern Trauzettel, Alexander Buzdin and Nimrod Stander for carefully reading of the manuscript. J.C. acknowledges the Geballe Laboratory for Advanced Materials at Stanford for hospitality during the completion of this work. This work was supported by the Institut Universitaire de France (Chair

of A. Buzdin), the Agence Nationale de la Recherche under grant ANR-07-NANO-011-05 (ELEC-EPR), the

MARCO/FENA program and the Air Force Office of Scientific Research.

- 
- \* Present address: Laboratoire Pierre Aigrain, Département de Physique de l'Ecole Normale Supérieure  
24 rue Lhomond, 75231 Paris Cedex 05, France
- <sup>1</sup> Ph. Avouris, Z. Chen and V. Perebeinos, *Nature Nano.* **2**, 605 (2007).
- <sup>2</sup> A.H. Castro Neto et al., arXiv:0709.1163.
- <sup>3</sup> C. W. Beenakker, *Rev. Mod. Phys.* **80**, 1337 (2008).
- <sup>4</sup> S. Heinze et al., *Phys. Rev. Lett.* **89**, 106801 (2002).
- <sup>5</sup> A. Javey et al., *Nano Lett.* **5**(2), 345 (2005).
- <sup>6</sup> B. Huard, N. Stander, J.A. Sulpizio, D. Goldhaber-Gordon, *Phys. Rev. B* **78**, 121402(R) (2008).
- <sup>7</sup> E.J.H. Lee et al., *Nature Nano.* **3**, 486 (2008).
- <sup>8</sup> H. Schomerus, *Phys. Rev. B* **76**, 045433 (2007).
- <sup>9</sup> Y.M. Blanter and I. Martin, *Phys. Rev. B* **76**, 155433 (2007).
- <sup>10</sup> L. DiCarlo, J.R. Williams, Y. Zhang, D.T. McClure, and C.M. Marcus, *Phys. Rev. Lett.* **100**, 156801 (2008).
- <sup>11</sup> R. Danneau et al., *Phys. Rev. Lett.* **100**, 196802 (2008).
- <sup>12</sup> G. Giovannetti et al., *Phys. Rev. Lett.* **101**, 026803 (2008).
- <sup>13</sup> L.D. Landau, *Course of Theoretical Physics, Quantum Mechanics*, (Pergamon press).
- <sup>14</sup> M.M. Fogler, D.S. Novikov, L.I. Glazman, and B.I. Shklovskii, *Phys. Rev. B* **77**, 075420 (2008).
- <sup>15</sup> N. Stander, B. Huard, and D. Goldhaber-Gordon, arXiv:0806.2319.
- <sup>16</sup> In the whole paper, we take the formal limit  $W/L \rightarrow \infty$  and express the results in terms of conductance per channel,  $W$  and  $L$  being respectively the width (along  $y$ ) and the length (along  $x$ ) of the graphene strip. In practice, this corresponds to samples with aspect ratio  $W/L \gtrsim 4$  according to Ref.<sup>30</sup>.
- <sup>17</sup> V.V. Cheianov, V.I. Falko, *Phys. Rev. B* **74**, 041403(R) (2006).
- <sup>18</sup> M.I. Katsnelson, K.S. Novoselov, and A.K. Geim, *Nature Phys.* **2**, 620 (2006).
- <sup>19</sup> T. Ando, T. Nakanishi and R. Saito, *JPSJ* **67**, 2857 (1998).
- <sup>20</sup> O. Klein, *Z. Phys.* **53**, 157 (1929).
- <sup>21</sup> B. Huard et al., *Phys. Rev. Lett.* **98**, 236803 (2007).
- <sup>22</sup> J.R. Williams, L. DiCarlo, and C.M. Marcus, *Science* **317**, 638 (2007).
- <sup>23</sup> B. Ozyilmaz et al., *Phys. Rev. Lett.* **99**, 166804 (2007).
- <sup>24</sup> J.B. Oostinga et al., *Nature Mat.* **7**, 151 (2008).
- <sup>25</sup> R. V. Gorbachev et al., arXiv:0804.2081.
- <sup>26</sup> G. Liu et al., *Appl. Phys. Lett.* **92**, 203103 (2008).
- <sup>27</sup> X. Du et al., *Nature Nanotechnology* **3**, 491 - 495 (2008).
- <sup>28</sup> K.I. Bolotin, K.J. Sikes, J. Hone, H.L. Stormer, and P. Kim, *Phys. Rev. Lett.* **101**, 096802 (2008).
- <sup>29</sup> A.F. Young and P. Kim, arXiv:0808.0855v2.
- <sup>30</sup> J. Tworzydło, B. Trauzettel, M. Titov, A. Rycerz, and C.W.J. Beenakker, *Phys. Rev. Lett.* **96**, 246802 (2006).
- <sup>31</sup> P. Kennedy, *J. Phys. A: Math. Gen.* **35**, 689-698 (2002).
- <sup>32</sup> C. W. Groth, J. Tworzydło, C. W. J. Beenakker, *Phys.Rev.Lett.* **100**, 176804 (2008).
- <sup>33</sup> P. San-Jose, E. Prada and D. S. Golubev, *Phys. Rev. B* **76**, 195445 (2007).
- <sup>34</sup> C.H. Lewenkopf, E.R. Mucciolo, and A.H. Castro Neto, *Phys. Rev. B* **77**, 081410(R) (2008).
- <sup>35</sup> J.H. Chen, C. Jang, S. Adam, M.S. Fuhrer, E.D. Williams and M. Ishigami, *Nature Phys.* **4**, 377 (2008).
- <sup>36</sup> P. Lafarge, PhD thesis, Université de Paris 6, p.32 (1993) <http://tel.archives-ouvertes.fr/tel-00195918>.
- <sup>37</sup> M. Abramowitz and I.A. Stegun, 15.3 and 15.5, *Handbook of Mathematical Functions with Formulas, Graphs, and Mathematical Tables*, (New York, Dover Publications).